ORIGINAL ARTICLE

Novel biosynthesized silver nanoparticles from cobweb as adsorbent for Rhodamine B: equilibrium isotherm, kinetic and thermodynamic studies

Luqmon Azeez[1] · Agbaje Lateef[2] · Segun A. Adebisi[1] · Abdulrasaq O. Oyedeji[3]

Abstract
This study has investigated the adsorption of Rhodamine B (Rh-B) dye on novel biosynthesized silver nanoparticles (AgNPs) from cobweb. The effects of contact time, initial pH, initial dye concentration, adsorbent dosage and temperature were studied on the removal of Rh-B and they significantly affected its uptake. Adsorption isotherms were evaluated using Langmuir, Freundlich, Temkin and Dubinin–Radushkevich isotherm models. The adsorption process was best described by Langmuir isotherm with R^2 of 0.9901, indicating monolayer adsorption. The maximum adsorption capacity (q_{max}) of 59.85 mg/g showed that it has relatively high performance, while adsorption intensity showed a favourable adsorption process. Pseudo-second-order kinetics fitted best the rate of adsorption and intra-particle diffusion revealed both surface adsorption and intra-particle diffusion-controlled adsorption process. Negative values of thermodynamic parameters ($\Delta H°$, $\Delta S°$ and $\Delta G°$) indicated an exothermic and spontaneous adsorption process. The mean sorption energy (E) and activation energy (E_a) suggested the uptake of Rh-B onto AgNPs was chemical in nature (chemosorption).

Keywords Biosynthesized AgNPs · Chemosorption · Adsorption isotherm · pH point of zero charge · Spontaneity of adsorption · Wastewater

Introduction

Demand for developmental strides and industrialization has led to more toxic effluents being discharged with little or no treatment into the environment especially water bodies. Quality water is indispensable and essential to life (Fawole et al. 2002) but meeting the quality for different purposes has been a huge task because of loads of wastes received by it from domestic, municipal and industrial sources (Lateef 2004; Adewoye and Lateef 2004; Pal and Deb 2014; Azeez

et al. 2015). Most of these wastes have detrimental effects on environment, human health, agricultural produce, aquatic lives and are also known to be genotoxic (Bakare et al. 2003; Lateef et al. 2007). Dyes are examples of such wastes and are increasingly being used in pharmaceutical, paint, textile industries and laboratories as indicators. They are non-biodegradable pollutants that affect water quality by causing foul odour, preventing light penetration, increasing chemical oxygen demand, decreasing dissolved oxygen level, and eventually leading to death of aquatic lives. They have been found to be nephrotoxic and also induce toxicity on reproductive system (Das et al. 2006, 2008; Baskaran et al. 2011; Chen et al. 2012; Ramalingam et al. 2015; Tan et al. 2015).

Rhodamine B (Rh-B) belongs to xanthene dyes and is highly soluble in water. It has high fastness and possesses fluorescent property. These characteristics have made it to be widely applicable in textile, glass, paint, paper, and leather dyeing (Das et al. 2006, 2008; Satapathy et al. 2013). However, it is carcinogenic causing hypothalamic cell apoptosis leading to hormonal imbalances. It has also been reported to cause eyes, skin, and respiratory tract irritations (Satapathy et al. 2013; Pal and Deb 2014; Bhattacharyya et al. 2014;

✉ Luqmon Azeez
  azeez012000@yahoo.com

1 Department of Chemical Sciences, Osun State University, Osogbo, Osun State, Nigeria

2 Nanotechnology Research Group (NANO+), Laboratory of Industrial Microbiology and Nanobiotechnology, Department of Pure and Applied Biology, Ladoke Akintola University of Technology, PMB 4000, Ogbomoso, Oyo State, Nigeria

3 Department of Science Laboratory Technology, Federal Polytechnic Ilaro, Ilaro, Ogun State, Nigeria

Sulistina et al. 2014; Shen et al. 2015; Mahmoud et al. 2015; Huang et al. 2016). Wastewater containing Rh-B, therefore, needs to be effectively, efficiently and qualitatively treated before being discharged into the environment (Inyinbor et al. 2015, 2016a, b).

Several studies have reported different methods for dye removal from aqueous solutions such as photochemical degradation, biological degradation, coagulation–flocculation, chemical oxidation, adsorption, membrane separation process, electrochemical, reverse osmosis, aerobic and anaerobic microbial degradation, but their shortcomings have limited their applications (Majumdar et al. 2015; Das et al. 2013; Sadaf and Bhatti 2014; Sadhukhan et al. 2014; Shen et al. 2015). Adsorption has proved to be the most effective physicochemical method in removing dye from effluents with activated carbon as the most widely used adsorbent. Activated carbon has been found useful, and effective in dye removal but high cost of preparation and regeneration maintenance have made its use economically burdensome (Tan and Hameed 2010; Giwa et al. 2015; Santhi and Kumar 2015). This has led to the use of effective alternative adsorbents such as hen feather (Mittal et al. 2007), cassava pellets (Okewale et al. 2013), perlite (Vijayakumar et al. 2012), *Rhizopus oyrzae* biomass (Das et al. 2006, 2008), *Mucor rouxii* (Majumdar et al. 2015) *Raphia hookeri* epicarp (Inyinbor et al. 2016a), Chitosan (Inyinbor et al. 2016b), silk (Jiwalak et al. 2010), phosphoric acid-modified rice husk (Dada et al. 2012) and sawdust of *Parkia biglobosa* (Giwa et al. 2015) for the removal of dyes. However, as microparticles, these materials will require long time for maximum adsorption.

Presently, the applications of metal nanoparticles as adsorbents have been on increase due to their morphology such as highly reactive sites, controlled size and high surface area. Multi-walled carbon nanotube (Yang and Xing 2010), MgO (Li et al. 2012; Mahmoud et al. 2015), chitosan–zinc oxide (Salehi et al. 2010), zero-valent iron (Satapanajaru et al. 2011), silver (Satapathy et al. 2013), gold (Xu, 2010), NiO (Samiey and Farhadi 2013), TiO_2 (Hsiao et al. 2014; Lyu et al. 2014) nanoparticles have been employed in wastewater purification and have proved to be faster in action and more effective in performance. Also, catalytic degradation of dyes has been achieved using nanoparticles (Bogireddy et al. 2015; Han et al. 2013; Kumari and Philip 2015; Lateef et al. 2016a, b, c; Ojo et al. 2016; Oladipo et al. 2017). Despite the excellent adsorptive capacity of nanoparticles, toxicity arising from their use has been of great concern. Nano-TiO_2 has limited adsorption affinity for anionic dyes, and was reported to cause unusual sedimentation, haemagglutination, haemolysis of erythrocytes in humans and physical changes to aquatic ecosystem (Li et al. 2008; Canesi et al. 2010). Nano-Fe_3O_4, nano-ZnO and nano-MgO were found

to be toxic to human lung alveolar epithelial cells, neurons as well as animal cells (Choi and Choy 2009; Lu et al. 2009; Zhao et al. 2009). Carbon nanotubes are reported to be toxic to human dermal fibroblast cells. This might not be unconnected with their methods of preparation which are chemical/reduction methods (Patlolla et al. 2010). To avoid toxicities arising from physical and chemical-based synthetic routes, green (biological) synthesis of nanoparticles which does not involve the use of hazardous chemicals provides effective route for non/less toxic and eco-friendly nanoparticles (Vanaja et al. 2014; Adelere and Lateef 2016; Lateef et al. 2016d, e; Pavya et al. 2016; Shukla and Iravani 2017).

In this study, novel eco-friendly silver nanoparticles biosynthesized from extracts of cobweb (as source of biomolecules that serve as reducing agents in reducing Ag^+ to zero-valent Ag^0 to form AgNPs) were used for the adsorption of Rhodamine B from aqueous solution.

Materials and methods

Biosynthesis and characterization of AgNPs

AgNPs used in this study were biologically synthesized from cobweb as earlier described (Lateef et al. 2016f). The scheme of the synthesis is shown in Fig. 1. Cobweb extract was prepared through hydrolysis of 0.1 g of washed and air-dried cobweb with 10 ml of 0.1 M NaOH at 90 °C for 1 h. The resulting liquid was centrifuged at 4000 rpm for 30 min to obtain the crude cobweb extract. Biosynthesis was carried by reacting 1 ml of cobweb extract with 40 ml of $AgNO_3$ under ambient condition. The biosynthesized AgNPs were characterized by UV–Vis spectroscopy, Fourier transform infrared spectroscopy (FTIR) and transmission electron microscopy (TEM) as previously described by Lateef et al. (2016f).

pH point of zero charge (pH$_{pzc}$)

The pH point of zero charge (pHpzc) was determined as previously reported (Giwa et al. 2015; Inyinbor et al. 2015). A weighed amount (0.1 g) of AgNPs was added to 50 ml of 0.1 M NaCl with predetermined pH in 250-ml conical flask. The pH of the resultant solution was adjusted between pH 2 and 10 with either 0.1 M NaOH or HCl. The conical flasks were sealed and shaken in an orbital shaker (Stuart SSLI, Barlword Scientific Ltd Britain) for 24 h, after which the final pH values were measured. The difference between the initial and final pH was calculated and plotted against the

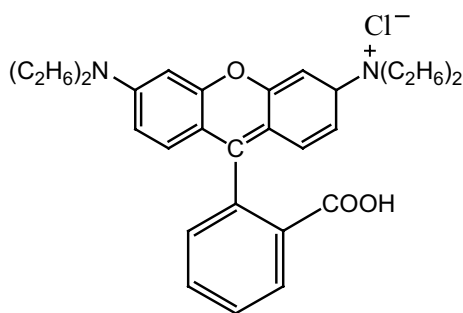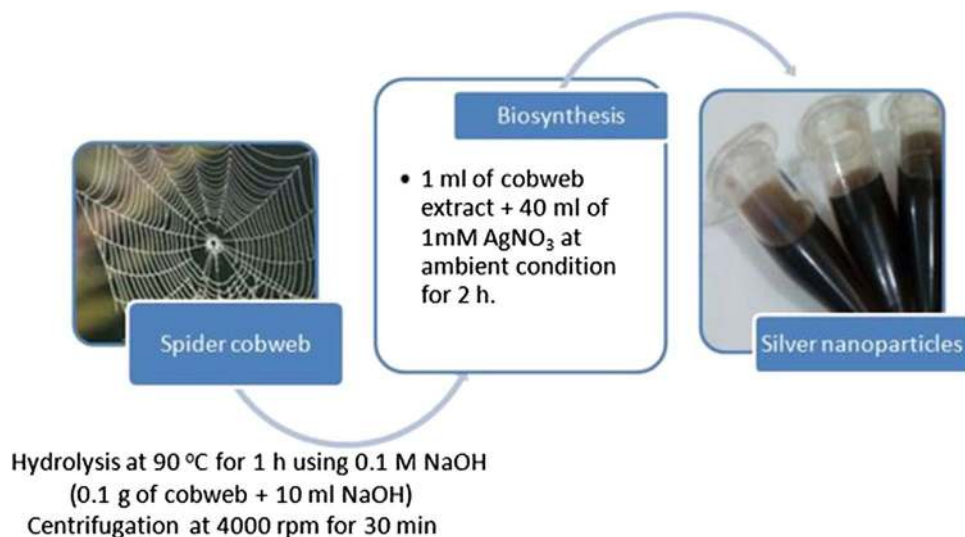**Fig. 1** Scheme for the biosynthesis of AgNPs using cobweb extract

Hydrolysis at 90 °C for 1 h using 0.1 M NaOH
(0.1 g of cobweb + 10 ml NaOH)
Centrifugation at 4000 rpm for 30 min

Fig. 2 Structure of Rhodamine B (Rh-B) dye (Inyinbor et al. 2015)

initial pH. pH$_{pzc}$ was obtained from the point of intersection with pH axis.

Adsorbate characteristics and preparation

The dye Rhodamine B (Fig. 2) with molecular formula $C_{28}H_{31}N_2O_3Cl$, λ_{max} 554 nm was purchased from Sigma-Aldrich (Germany) and was used without further purification. All other reagents were of analar grade. A stock solution of Rhodamine B (Rh-B) was prepared by dissolving 0.1 g in 1000 ml deionized–distilled water.

Adsorption studies

Effects of initial solution pH (1–9), contact time (5–60 min), AgNPs dosage (0.2–1 g/l), initial Rh-B concentration of dye (10–50 mg/l) and temperature (303–333 K) on the adsorption of Rh-B on AgNPs were studied in batches. The pH of the Rh-B solution was adjusted with 0.1 M HCl or 0.1 M NaOH. 1 g/l of AgNPs was weighed and added to 100 ml of 50 mg/l Rh-B solution in a 250-ml conical flask. The flask was shaken in a thermostat-regulated water bath shaker

(Uniscope water bath shaker) at 30 °C, agitated at 150 rpm for 30 min. The solution was centrifuged at 1500 rpm. The pH was measured with Jenway 3505 pH meter. The concentration of unadsorbed dye was determined using a Jenway 6405 UV–Visible spectrophotometer (Buch Scientific Inc. USA) at 554 nm. Percentage removal and quantity adsorbed at a given time t were calculated using the following equations:

$$\% \text{ Removal} = \frac{\left(C_i - C_f\right) \times 100}{C_i} \qquad (1)$$

$$q_t = \frac{(C_i - C_t)V}{M} \qquad (2)$$

where q_t is the amount of dye adsorbed per unit mass of adsorbent (mg/g), C_i is the initial dye concentration (mg/l), C_f is the final dye concentration (mg/l), C_t is the residual concentration at time t, V is the volume of dye solution (l) and M mass of adsorbent (g).

Adsorption isotherms

Adsorption isotherms were studied on the adsorption of Rh-B on AgNPs with Langmuir (Eqs. 3 and 3a), Freundlich (Eq. 4), Tempkin (Eqs. 5 and 5a) and Dubinin–Radushkevich (Eqs. 6, 6a and 6b) adsorption models.

The Langmuir isotherm is a monolayer type of adsorption which assumes that adsorption process takes place uniformly within the adsorbent surface and with uniform distribution of energy level (Langmuir 1918). Freundlich isotherm explains the heterogeneous nature of adsorption sites having non-uniform distribution of energy level (Freundlich 1906). Tempkin isotherm explains the influences of indirect adsorbate/adsorbent interactions on

adsorption isotherms and also explains the interactions of these with the heat of adsorption (Tempkin and Pyzhev 1940). The Dubinin–Radushkevich model explains the relationship between energy of adsorption and type of adsorption process involved (Dubinin and Radushkevich 1947).

$$\frac{C_e}{q_e} = \frac{Ce}{q\text{max}} + \frac{1}{q\text{max} K_L} \tag{3}$$

$$R_L = \frac{1}{1 + K_L C_o} \tag{3a}$$

$$\log q_e = \frac{1}{n} \log C_e + \log K_f \tag{4}$$

$$q_e = B \ln A + B \ln C_e \tag{5}$$

$$B = \frac{RT}{b} \tag{5a}$$

$$\ln q_e = \ln q_o - \beta \varepsilon^2 \tag{6}$$

$$\varepsilon = RT \ln \left(1 + \frac{1}{C_e}\right) \tag{6a}$$

$$E = \sqrt{1/2\beta} \tag{6b}$$

where C_e is the equilibrium concentration of Rh-B dye (mg/l), q_e is the quantity of Rh-B dye adsorbed onto the AgNPs at equilibrium (mg/g), q_{max} is the maximum monolayer adsorption capacity of adsorbent (mg/g) and K_L is the Langmuir adsorption constant (l/mg).

A graph of $\frac{Ce}{qe}$ against C_e should give a straight line graph with the slope $\frac{1}{q\text{max}}$ and $\frac{1}{q\text{max} K_L}$ as intercept. The value of R_L is in the range $0 < R_L < 1$ indicating whether the adsorption is favourable or not: unfavourable ($R_L > 1$), linear ($R_L = 1$) or irreversible ($R_L = 0$).

K_f and n are Freundlich constants corresponding to adsorption capacity and adsorption intensity or surface heterogeneity, respectively. They are obtained from linear plot of $\log q_e$ versus $\log C_e$ with the slope $\frac{1}{n}$ and intercept $\log K_f$.

A (l/g) and B are Tempkin isotherm and Tempkin constants, respectively, which are obtained from the plot of q_e against $\ln C_e$. The value of b (J/mol) which is related to the heat of absorption is calculated using Eq. (5a), T is the absolute temperature (K), and R is the gas constant (8.314 J/mol$^/$K).

The value of E in Dubinin–Radushkevich (D–R) model gives information about the type of adsorption whether chemical or physical involved during the uptake of Rh-B

by AgNPs. A linear graph of $\ln q_e$ against ε gives a slope of β and intercept of $\ln q_o$.

Adsorption kinetics

Adsorption kinetics were studied with pseudo-first-order (Eq. 7), pseudo-second-order (Eq. 8), Elovich kinetic models (Eq. 9) and intra-particle diffusion model (Eq. 10). Adsorption kinetics were validated with non-linear Chi-square test (Eq. 11) and correlation coefficient. Boyd model (Eqs. 12 and 13) was used to further confirm rate controlling step of adsorption process.

$$\ln(q_e - q_t) = \ln q_e - K_1 t \tag{7}$$

$$\frac{t}{q_t} = \frac{1}{K_2 q_e^2} + \frac{t}{q_e} \tag{8}$$

$$q_t = \frac{1}{\beta} \ln(\alpha\beta) + \frac{1}{\beta} \ln t \tag{9}$$

$$q_t = K_{diff} t^{1/2} + C \tag{10}$$

$$X^2 = \sum_{i=1}^{n} \frac{(q_{exp} - q_{cal})^2}{q_{cal}} \tag{11}$$

$$F = \frac{q_t}{q_e} \tag{12}$$

$$B_t = -0.4977 - \ln(1 - F) \tag{13}$$

where q_e is the quantity adsorbed at equilibrium (mg/g) and q_t is the quantity absorbed at time t (mg/g) and K_1 is the rate constant for the pseudo-first-order sorption in min^{-1} obtained from the plot of $\ln(q_e - q_t)$ against t, t is time for adsorption in min.

K_2 is the rate constant of the pseudo-second-order kinetic model in g/mg/min obtained for the plot of $\frac{t}{q_t}$ against t. K_{diff} is the rate constant of intra-particle diffusion (mg/g min$^{-1/2}$). α and β are constants depicting chemosorption rate and the extent of surface coverage respectively, which are obtainable from the plot of q_t against $\ln t$.

F is the fraction of solute adsorbed at any time t. B_t is a mathematical function of F.

Adsorption thermodynamics

Thermodynamic parameters that explain spontaneity, energetics and the nature of adsorbate–adsorbent interactions are calculated using the following equations:

$$\ln K_o = \frac{\Delta S^o}{R} - \frac{\Delta H^o}{RT} \tag{14}$$

$$\Delta G^o = -RT \ln K_o \tag{15}$$

$$S^* = (1 - \theta)e^{-E_a/RT} \tag{16}$$

$$\theta = 1 - \frac{C_e}{C_o} \tag{17}$$

K_o is calculated from q_e/C_e, T is temperature (K), R is gas constant. ΔS^o is change in entropy and ΔH^o is change in enthalpy obtained from the plot of $\ln K_o$ against $\frac{1}{T}$. ΔG^o, change in free energy is calculated using Eq. (15). E_a is activation energy which is obtained from the plot of $(1 - \theta)$ against $\frac{1}{T}$. S^* is the sticking probability which is a function of adsorbate–adsorbent system and its value ranges between $0 < S^* < 1$.

Results and discussion

Biosynthesized AgNPs

The pH of biosynthesized AgNPs was 6.72 and pH_{pzc} was 7.82 (Fig. 3) which was fairly neutral. pH_{pzc} is a parameter used to express the degree of adsorbent surface ionization. At a pH below pH_{pzc} of the adsorbent, the surface of the adsorbent is positively charged and attracts anions while at pH above it, the surface of the adsorbent is negatively charged and attracts cations (Giwa et al. 2015; Torres et al. 2007). Earlier data revealed that cobweb extract-mediated AgNP biosynthesis gave dark brown nearly spherical crystalline AgNPs with surface plasmon resonance obtained at 436 nm. The polydispersed particles having size range of 3–50 nm were formed due to the activities of proteinous materials in the cobweb extract (Lateef et al. 2016f). The AgNPs mediated by cobweb extract have shown
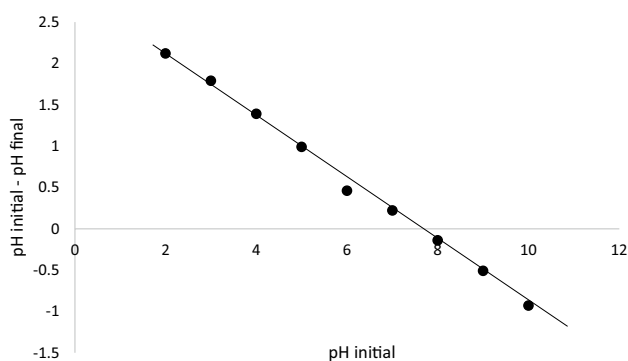
tremendous activities; including antimicrobial (Lateef et al. 2016f), desulphurization (Olajire et al. 2017), hydrogen peroxide scavenging, anticoagulant and thrombolytic applications (Lateef et al. 2017). However, until now, there is no report on the use of cobweb-mediated AgNPs for the removal of dyes.

Effect of initial pH on the adsorption of Rh-B on AgNPs

Effect of various pH on adsorption of Rh-B on AgNPs is presented in Fig. 4. Adsorption process is dependent on pH where a change would either increase or reduce percentage adsorption. pH influences the charge on the surface of adsorbent and mobility of adsorbate (Majumdar et al. 2015; Das et al. 2013; Giwa et al. 2015). Percentage removal of Rh-B increased from 72 to 78% with increase in pH from pH 2 to 3.4 where maximum adsorption was observed. This decreased to the minimum (55%) at pH 9. At a pH below 7.82 (pH_{pzc} for AgNPs), the surface of AgNPs was highly cationic, while Rh-B surface at pH less than 3.22 was also cationic, thus caused repulsion between adsorbent and adsorbate resulting in poor rate of adsorption. But as the pH increased especially at pH 3.4 (which is above 3.22 for Rh-B), the surface of Rh-B became anionic, therefore, resulting to high rate of adsorption. This could be due to electrostatic interaction between cationic adsorbent and anionic adsorbate leading to favourable adsorption of Rh-B (Majumdar et al. 2015; Das et al. 2013). With increase in pH, the surface of AgNPs became less cationic as it was nearing its pHpzc and thereafter became anionic at pH above it. This was responsible for reduction in rate of adsorption obtained at pH above 7.82. Similar trends have been
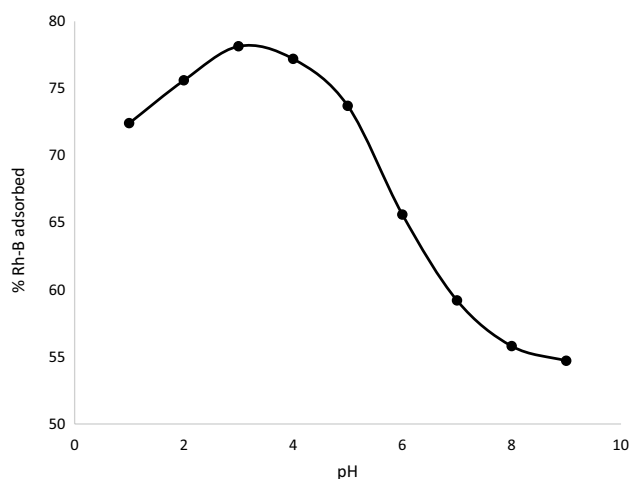
Fig. 3 pH point of zero charge (pHpzc)

Fig. 4 Effect of different pH on the adsorption of Rh-B on AgNPs. 1 g/l of AgNPs in 100 ml of 50 mg/l Rh-B, agitation speed 150 rpm, agitation time 30 min, temp. 303 K

previously reported in different studies (Giwa et al. 2015; Inyinbor et al. 2015; Ramalingam et al. 2015). Consequently, all batch adsorption experiments were, therefore, carried out at pH 3.4.

Effects of initial concentrations of Rh-B

The result of effect of initial dye concentrations on percentage uptake of Rh-B on AgNPs is presented in Fig. 5. It was discovered from the plot that percentage removal of Rh-B increased with increasing concentration of the dye. Maximum adsorption of 93% was recorded for highest concentration (50 mg/l), while the least adsorption (67%) was obtained for lowest concentration (10 mg/l). This could be attributed to the increase in the driving force from higher concentration which enhances the sorption process as earlier reported (Inyinbor et al. 2016a, b; Satapathy et al. 2013).

Effect of contact time

Contact time is one of the most effective factors in batch adsorption process and its effect on the adsorption of Rh-B on AgNPs is presented in Fig. 6. It is evident from the plot that the adsorption capacity (q_t) at time t increased steadily with increase in time until it reached equilibrium at 30 min. The increase was from 7 mg/g at 5 min to 30.55 mg/g at 30 min. This is in agreement with earlier reports (Amuda et al. 2014; Mahmoud et al. 2015) where the noticed action could be due to the available surface sites before equilibrium was reached.

Effect of adsorbent dosage

The result of effect of AgNPs dosage on the removal of Rh-B from aqueous solution is presented in Fig. 7. Percentage Rh-B adsorbed increased with increase in AgNPs dosage
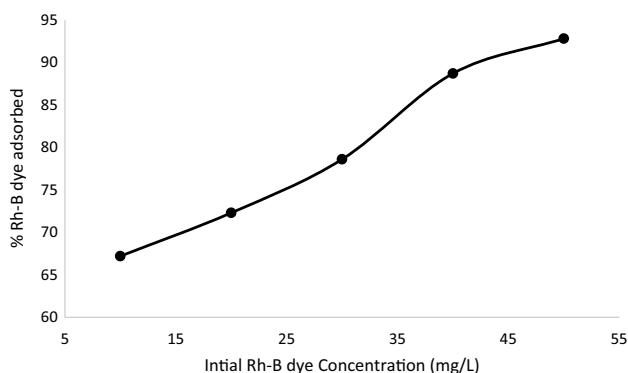
Fig. 6 Adsorption capacity of AgNPs for the removal of Rh-B at different contact times. 1 g/l of AgNPs in 100 ml of 50 mg/l Rh-B, agitation speed—150 rpm at 303 K, pH 3.4

from 0.2 to 1 g/l. The increase was from 52 to 87%. The increase in the percentage removal with adsorbent dosage may be adduced to the increase in the nanoparticle's surface area available for adsorption. This is in consonance with earlier reports (Satapathy et al. 2013; Amuda et al. 2014; Inyinbor et al. 2016a, b).

Effect of temperature

Temperature influences adsorption capacity and its effect on the adsorption of Rh-B onto AgNPs is presented in Fig. 8. The temperature dependency of adsorption of Rh-B on AgNPs was studied at 303, 313, 323, 333 K, and it was observed that percentage removal of Rh-B reduced with increase in temperature. This phenomenon indicates that the adsorption process was exothermic in nature and it is in consonance with earlier reports (Satapathy et al. 2013; Girish and Murty 2014; Inyinbor et al. 2016a, b).

Fig. 5 Percentage removal of Rh-B on AgNPs at different concentrations. 1 g/l of AgNPs in 100 ml of 50 mg/l Rh-B, agitation speed—150 rpm, agitation—30 min at 303 K, pH 3.4
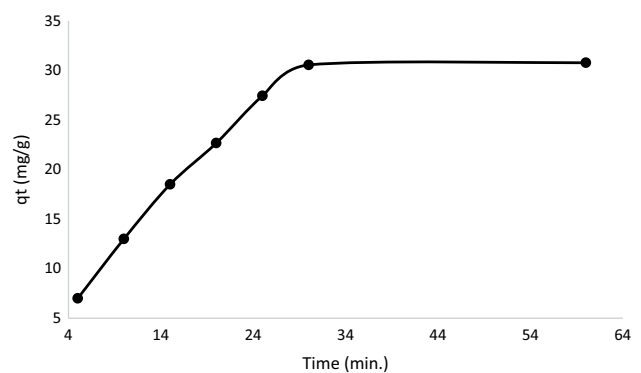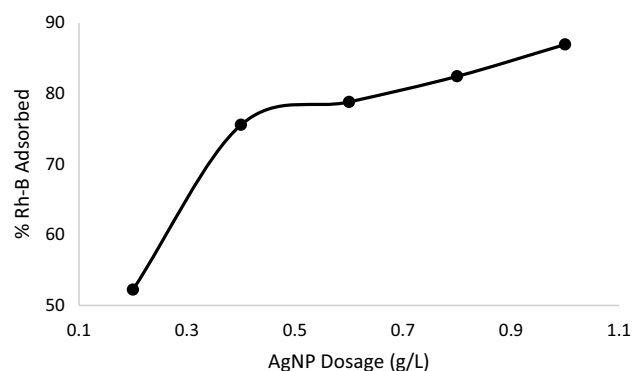
Fig. 7 Effect AgNPs dosage on the adsorption of Rh-B. 50 mg/l Rh-B, agitation speed—150 rpm, agitation time—30 min at 303 K, pH 3.4
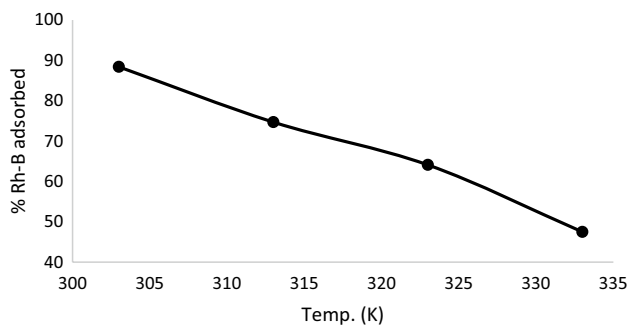
Fig. 8 Effect of temperature on the adsorption of Rh-B on AgNPs at different temperatures. 1 g/l of AgNPs in 100 ml of 50 mg/l Rh-B, 150 rpm 60 min, pH 3.4
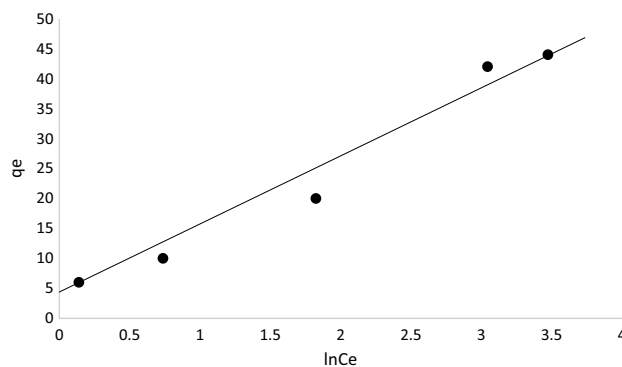

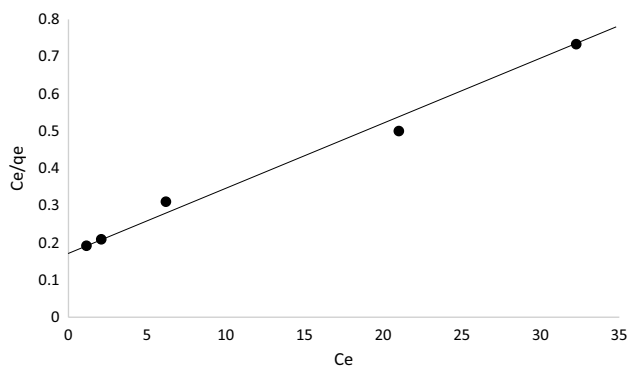**Fig. 11** Temkin adsorption isothermal plot for the adsorption of Rh-B on AgNPs

Fig. 9 Langmuir adsorption isothermal plot for the adsorption of Rh-B on AgNPs
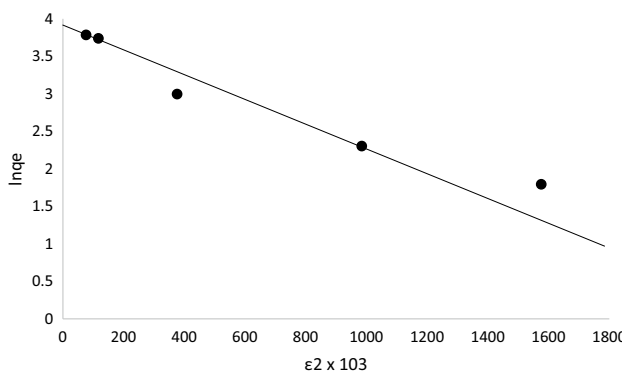

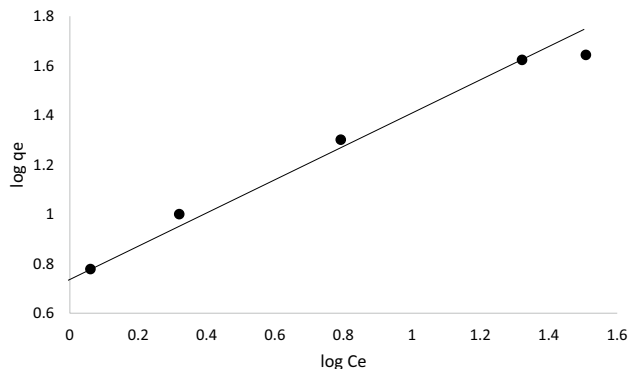**Fig. 12** Dubinin–Radushkevich adsorption isothermal plot for the adsorption of Rh-B on AgNPs

Fig. 10 Freundlich adsorption isothermal plot for the adsorption of Rh-B on AgNPs

Adsorption isotherms

For the explicit examination of the relationship between quantity of Rh-B adsorbed and its concentration, Langmuir, Freundlich, Tempkin and Dubinin–Radushkevich isothermal models were employed. Figures 9, 10, 11 and 12 show the

plots of Langmuir, Freundlich, Tempkin and Dubinin–Radushkevich adsorption isotherms, respectively, for the adsorption of Rh-B on AgNPs. The parameters obtained from the plots are presented in Table 1. Correlation coefficient (R^2) was used to determine which model best describes the adsorption process. The closer the R^2 to unity (1), the better the agreement between experimental data, and model predicted value and the best fit it is. Comparing R^2 of each isotherm, Langmuir (0.9901), Freundlich (0.9860), Tempkin (0.9740) and Dubinin–Radushkevich (0.9441), it is evident that Langmuir isotherm best fits the adsorption of Rh-B on AgNPs which indicates monolayer and homogenous adsorption process with all adsorption sites possessing equal affinity for adsorbate (Foo and Hameed 2010). The favourability of the adsorption process is confirmed if the value of R_L is in the range $0 < R_L < 1$. As obtained in this study (Table 1), R_L is 0.18, confirming that the adsorption process was favourable (Majumdar et al. 2015; Satapathy et al. 2013; Inyinbor et al. 2016a, b).

The maximum monolayer adsorption (q_{max}) obtained from Langmuir plot is 59.85 mg/g and when compared with

Table 1 Adsorption isotherm parameters for the uptake of Rh-B on AgNPs at 30 °C

Isotherms	Constants	Values
Langmuir	q_{max} (mg/g)	59.85
	K_L (l/mg)	0.093
	R_L	0.18
	R^2	0.9901
Freundlich	n	1.647
	K_F	6.07
	R^2	0.9860
Temkin	B	12.21
	A (l/g)	1.48
	b (J/mol)	206.32
	R^2	0.9740
Dubinin–Radushkevich	q_o (mg/g)	42.81
	β (mol²/KJ²)	0.00133
	E (KJ/mol)	19.38
	R^2	0.9441

previously published reports in other studies (Table 2), it shows that AgNPs is a relatively better adsorbent in terms of performance than some previously used adsorbents (Majumdar et al. 2015; Das et al. 2006; Satapathy et al. 2013; Amuda et al. 2014; Inyinbor et al. 2015, 2016a; Mahmoud et al. 2015; Shen et al. 2015).

K_f and n were calculated from Freundlich isotherm plot with the value of n (1.647) greater than 1 indicating a favourable adsorption of Rh-B on AgNPs and the chemical nature of adsorption (Foo and Hameed 2010; Amuda et al. 2014).

Adsorption energy (E) calculated from slope of Dubinin–Radushkevich plot is 19.38 kJ/mol suggesting that chemosorption was involved in the uptake of Rh-B on AgNPs as it was earlier reported (Inyinbor et al. 2015, 2016a, b).

Table 2 Comparison of monolayer adsorption capacity of Rh-B on AgNPs with other adsorbents

Adsorbent	q_{max} (mg/g)	References
Lantana camara stem	19.84	Amuda et al. (2014)
Raw dika nut	212.77	Inyinbor et al. (2015)
Dika nut char	52.90	(Inyinbor et al. 2016a, b)
MgO nanocomposite	77.2	Mahmoud et al. (2015)
NiO nanoparticle	52.91	Satapathy et al. (2013)
Plant-mediated AgNPs	1.891	Shen et al. (2015)
Rhizopus oryzae biomass	39.21	Das et al. (2006)
Mucor rouxii	74.6	Majumdar et al. (2015)
Cobweb-mediated AgNPs	59.85	This study

Adsorption kinetics

The rate of removal of Rh-B and its controlling mechanism were studied as part of kinetics. Pseudo-first-order, pseudo-second-order, Elovich kinetic models and intra-particle diffusion model were employed to describe Rh-B uptake onto AgNPs. The parameters obtained for pseudo-first-order, pseudo-second-order, Elovich kinetic models and intra-particle diffusion model are presented in Table 3. Correlation coefficient (R^2) was used to determine the goodness of fit between experimental and calculated data. R^2 of the best fit model must be the closest to 1. Also, similarities between experimentally determined and calculated data expressed using non-linear Chi-square test (χ^2) (Eq. 11) must exist. A relatively low (χ^2) value indicates the model successfully describes the equilibrium kinetics (Al-Meshragi et al. 2008; Boulinguiez et al. 2008). Comparison of correlation coefficients of pseudo-first-order ($R^2 = 0.9421$), pseudo-second-order ($R^2 = 0.9882$) and Elovich ($R^2 = 0.9723$) kinetic models shows that pseudo-second-order best describes the mechanism and rate of uptake of Rh-B on AgNPs. Equally, lower value of χ^2 validates pseudo-second-order as the kinetic model describing the rate of adsorption. This suggests that the controlling process of adsorption of Rh-B on AgNPs may be by chemosorption (Girish and Murty 2014).

Many factors control the rate of adsorption, one of which is intra-particle diffusion. The possibility of involvement of intra-particle diffusion affecting the adsorption process was studied and is presented in Fig. 13. To further investigate rate controlling step in the adsorption process, the Boyd model as given in Eqs. 12 and 13 was used and the result

Table 3 Adsorption kinetics of Rh-B on AgNPs

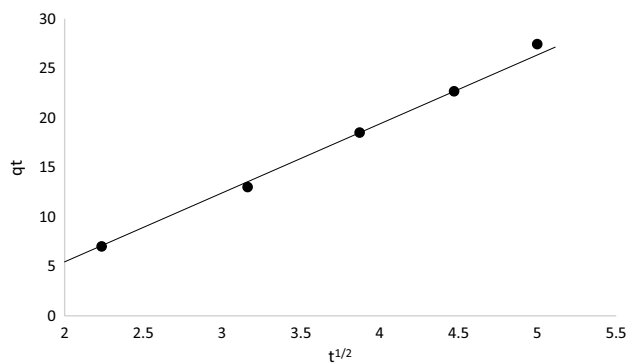|	
$q_{e\ experimental}$ (mg/g)	30.55
Pseudo-first order	
$q_{e,\ calculated}$ (mg/g)	33.44
K_1 (min⁻¹)	0.096866
R^2	0.942067
χ^2	0.249
Pseudo-second order	
$q_{e,\ calculated}$ (mg/g)	31.27
K_2 (g/mg/min)	0.000152
R^2	0.988223
χ^2	0.017
Elovich	
B (mg/g/min)	0.088
A (g/mg)	19.49
R^2	0.972226
Intraparticle diffusion	
K_{diff} (mg/g min⁻¹ᐟ²)	7.008
C (mg/g)	5.12

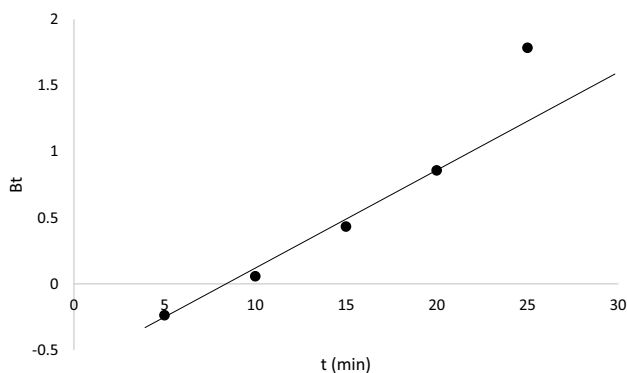**Fig. 13** Intra-particle diffusion of adsorption of Rh-B on AgNPs

Fig. 14 Boyd plot for adsorption of Rh-B on AgNPs

is presented in Fig. 14. The parameters obtained from the plot in Fig. 13 are presented in Table 3. A single linear plot obtained for intra-particle diffusion of AgNP–Rh-B did not pass through the origin and has high correlation coefficient ($R^2 = 0.9971$) indicating that intra-particle diffusion was involved in the adsorption but it was not the sole rate-controlling step. This was confirmed by Boyd plot which also did not pass through the origin. Therefore, surface adsorption and intra-particle diffusion were both concurrently occurring during adsorption process (Cheung et al. 2007; Hameed et al. 2008; Abou-Gamra and Medien 2013; Girish and Murty 2014). The value of C (intercept) gives the idea about the thickness of the boundary, the larger the value of C, the greater the boundary layer diffusion effect (Konicki et al. 2013).

Activation energy and adsorption thermodynamic

Thermodynamic parameters ($\Delta G°$, $\Delta H°$ and $\Delta S°$) calculated from Van't Hoff's plot (Fig. 15) for adsorption of Rh-B on AgNPs are presented in Table 4. These parameters give information about the spontaneity of adsorption process
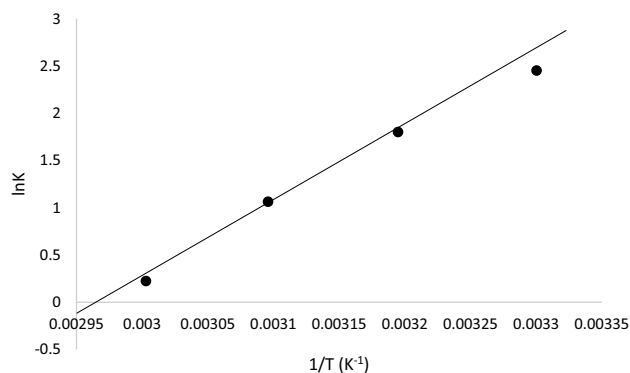

Fig. 15 Van't Hoff's plot for adsorption of Rh-B on AgNPs. 1 g/l of AgNPs in 100 ml of 50 mg/l Rh-B, 150 rpm 60 min, pH 3.4

(Satapathy et al. 2013). Activation energy (E_a) of the adsorption process obtained using Eqs. 16 and 17 is presented in Table 4. The magnitude of activation energy gives idea about the type of adsorption, which mainly can either be physiosorption or chemosorption (Mahmoud et al. 2015).

The E_a of the adsorption calculated was 103.273 kJ/mol which depicts the adsorption process as chemosorption because its range for chemosorption is usually between 40 and 800 kJ/mol. (Satapathy et al. 2013; Mahmoud et al. 2015).

Negative enthalpy ($-\Delta H°$) and entropy ($-\Delta S°$) values obtained indicate the adsorption process was exothermic in nature with decreased randomness during adsorption. The $\Delta G°$ values calculated at all temperatures were negative indicating the adsorption was spontaneous and feasible. The adsorption process became less spontaneous with higher values of $\Delta G°$ at higher temperature (Majumdar et al. 2015; Inyinbor et al. 2015; Mahmoud et al. 2015).

Conclusion

This study has reported the adsorption of Rh-B onto AgNPs biosynthesized using cobweb extract. Initial pH, contact time, initial dye concentration, adsorbent dosage and temperature significantly affected the adsorption of Rh-B and maximum adsorption was observed at pH 3.4. Four adsorption isotherms were used to describe the adsorption process with Langmuir isotherm suitably fitted best. Maximum monolayer adsorption capacity showed a relatively high performance. Pseudo-second-order kinetics best fitted the rate of adsorption which was both controlled by intra-particle diffusion and surface adsorption. Thermodynamic parameters indicated exothermic spontaneous adsorption process. The adsorption process was found to be chemical in nature as showed by the values of energy

Table 4 Thermodynamic parameters of Rh-D adsorption on AgNPs

Temperature (K)	$\Delta G°$ (KJ/mol)	$\Delta H°$ (KJ/mol)	$\Delta S°$ (JK/mo)	Ea (KJ/mo)	S
303	− 6.17	− 62.11	− 184.01	103.273	1.59×10^{-20}
313	− 4.54				
323	− 2.68				
333	− 0.56				

of adsorption and activation energy. This study has shown that low-cost and eco-friendly biosynthesized AgNPs with 93% dye removal from aqueous solution possess potential adsorbent capacity to remove dye.

References

Abou-Gamra ZM, Medien HAA (2013) Kinetic, thermodynamic and equilibrium studies of Rhodamine B adsorption by low cost biosorbent sugar cane bagasse. Eur Chem Bull 2:417–422

Adelere IA, Lateef A (2016) A novel approach to the green synthesis of metallic nanoparticles: the use of agro-wastes, enzymes and pigments. Nanotechnol Rev 5:567–587

Adewoye SO, Lateef A (2004) Assessment of the microbiological quality of *Clarias gariepinus* exposed to an industrial effluent in Nigeria. Environmentalist 24:249–254

Al-Meshragi M, Ibrahim HG, Aboabboud MM (2008) Equilibrium and kinetics of chromium adsorption on cement kiln dust. In: Proceedings of the World Congress on Engineering and Computer Science. WCECS, October 22–24, San Francisco, USA

Amuda OS, Olayiwola AO, Alade AO, Farombi AG, Adebisi SA (2014) Adsorption of methylene blue from aqueous solution using steam-activated carbon produced from L*antana camara* stem. J Environ Protect 5:1352–1363

Azeez L, Salau AK, Adewuyi SO, Osineye SO, Tijani KO, Balogun RO (2015) Safety evaluation of Osun river water containing heavy metals and volatile organic compounds (VOCs) in rats. Niger J Physiol Sci 30:103–109

Bakare AA, Lateef A, Amuda OS, Afolabi RO (2003) The aquatic toxicity and characterization of chemical and microbiological constituents of water samples from Oba River, Odo-Oba, Nigeria. Asian J Microbiol Biotechnol Environ Sci 5:11–17

Baskaran K, Venkatraman BR, Hema M, Arivoli S (2011) Adsorption kinetics and thermodynamics of malachite green dye onto *Calatropis gigantis* bark carbon. J Ind Pollut Control 27:5–13

Bhattacharyya KG, SenGupta S, Sarma GK (2014) Interactions of the dye, Rhodamine B with kaolinite and montmorillonite in water. Appl Clay Sci 99:7–17

Bogireddy NKR, Anand KKH, Mandal BK (2015) Gold nanoparticles-Synthesis by *Sterculia acuminata* extract and its catalytic efficiency in alleviating different organic dyes. J Mol Liq 211:868–875

Boulinguiez B, LeCloirec P, Wolbert D (2008) Revisiting the determination of Langmuir parameters application to tetrahydrothiophene adsorption onto activated carbon. Langmuir 24:6420–6424

Canesi L, Fabbri R, Gallo G, Vallotto D, Marcomini A, Pojana G (2010) Biomarkers in *Mytilus galloprovincialis* exposed to suspensions of selected nanoparticles (Nanocarbon black, C60 fullerene, nano-TiO$_2$, nano-SiO$_2$). Aquat Toxicol 100:168–177

Chen X, Xue Z, Yao Y, Wang W, Zhu F, Hong C (2012) Oxidation degradation of Rhodamine B in aqueous by UV/S$_2$O$_8^{2-}$ treatment system. Int J Photoenergy. https://doi.org/10.1155/2012/754691

Cheung WH, Szeto YS, McKay G (2007) Intraparticle diffusion processes during acid dye adsorption onto chitosan. Bioresour Technol 98:2897–2904

Choi SJ, Oh JM, Choy JH (2009) Toxicological effects of inorganic nanoparticles on human lung cancer A549 cells. J Inorg Biochem 103:463–471

Dada AO, Olalekan AP, Olatunya AM, Dada O (2012) Langmuir, Freundlich, Temkin and Dubinin–Radushkevich isotherms studies of equilibrium sorption of Zn2+ unto phosphoric acid modified rice husk. J Appl Chem 3:38–45

Das SK, Bhowal J, Das AR, Guha AK (2006) Adsorption behaviour of Rhodamine B on *Rhizopus oryzae* biomass. Langmuir 22:7265–7272

Das SK, Ghosh P, Ghosh I, Guha AK (2008) Adsorption of rhodamine B on *Rhizopus oryzae*: role of functional groups and cell wall components. Colloids Surf B Biointerf 65:30–34

Das SK, Khan MMR, Paranthamon T, Laffir F, Guha AK, Sekaran G, Mandal AB (2013) Nano-silica fabricated with silver nanoparticles: antifouling adsorbent for efficient dye removal, effective water disinfection and biofouling control. Nanoscale 5:5549–5560

Dubinin MM, Radushkevich LV (1947) The equation of the characteristic curve of the activated charcoal. Proc Acad Sci USSR Phys Chem Sect 55:331–337

Fawole OO, Lateef A, Amaefuna M (2002) Microbiological examination of drinking water in Ogbomoso metropolis, Southwest, Nigeria. Sci Focus 1:16–20

Foo KY, Hameed BH (2010) Insights into the modelling of adsorption isotherm systems. Chem Eng J 156:2–10

Freundlich HMF (1906) Over the adsorption in solution. J Phys Chem 57:385–470

Girish CR, Murty VR (2014) Adsorption of Phenol from aqueous Solution using *Lantana camara*, forest waste: kinetics, isotherm, and thermodynamic studies. Int Sch Res Notices. https://doi.org/10.1155/2014/201626

Giwa AA, Oladipo MA, Abdulsalam KA (2015) Adsorption of Rhodamine B from single, binary and ternary dye systems using Sawdust of *Parkia biglobosa* as adsorbent: isotherm, kinetics and thermodynamics studies. J Chem Pharm Res 7(2):454–475

Hameed BH, Tan IAW, Ahmad AL (2008) Adsorption isotherm, kinetic modeling and mechanism of 2,4,6-trichlorophenol on coconut husk-based activated carbon. Chem Eng J 144:235–244

Han TH, Khan MM, Kalathil S, Lee J, Cho MH (2013) Simultaneous enhancement of methylene blue degradation and power generation in a microbial fuel cell by gold nanoparticles. Ind Eng Chem Res 52:8174–8181

Hsiao Y-C, Wu T-F, Wang Y-S, Hu C-C, Huang C (2014) Evaluating the sensitizing effect on the photocatalytic decoloration of dyes using anatase-TiO$_2$. Appl Catal B 148–149:250–257

Huang Y, Zheng X, Feng S, Guo Z, Liang S (2016) Enhancement of rhodamine B removal by modifying activated carbon developed from *Lythrum salicaria* L. with pyruvic acid. Colloids Surf A 489:154–162

Inyinbor AA, Adekola FA, Olatunji GA (2015) Adsorption of Rhodamine B dye from aqueous solution on *Irvingia gabonensis* biomass: kinetics and thermodynamics studies. South Afr J Chem 68:115–125

Inyinbor AA, Adekola FA, Olatunji GA (2016a) Kinetics and isothermal modelling of liquid phase adsorption of Rhodamine B onto urea modified *Raphia hookerie* epicarp. Appl Water Sci. https://doi.org/10.1007/s13201-016-0471-7

Inyinbor AA, Adekola FA, Olatunji GA (2016b) Liquid phase adsorptions of Rhodamine B dye onto raw and chitosan supported mesoporous adsorbents: isotherms and kinetics studies. Appl Water Sci. https://doi.org/10.1007/s13201-016-0405-4

Jiwalak N, Rattanaphani S, Bremner JB, Rattanaphani V (2010) Equilibrium and kinetic modelling of the adsorption of indigo carmine onto silk. Fiber Polym 11:572–579

Konicki W, Sibera D, Mijowska E, Lendzion-Bielun Z, Narkiewicz U (2013) Equilibrium and kinetic studies on acid dye Acid Red 88 adsorption by magnetic $ZnFe_2O_4$ spinel ferrite nanoparticles. J Colloid Interf Sci 398:152–160

Kumari MM, Philip D (2015) Degradation of environment pollutant dyes using phytosynthesized metal nanocatalysts. Spectrochim Acta Part A Mol Biomol Spectr 135:632–638

Langmuir I (1918) The adsorption of gases on plane surfaces of glass, mica and platinum. J Am Chem Soc 40:1361–1403

Lateef A (2004) The microbiology of a pharmaceutical effluent and its public health implications. World J Microbiol Biotechnol 20:167–171

Lateef A, Yekeen TA, Ufuoma PE (2007) Bacteriology and genotoxicity of some pharmaceutical wastewaters in Nigeria. Int J Environ Health 1:551–562

Lateef A, Ojo SA, Folarin BI, Gueguim-Kana EB, Beukes LS (2016a) Kolanut (*Cola nitida*) mediated synthesis of silver-gold alloy nanoparticles: antifungal, catalytic, larvicidal and thrombolytic applications. J Clust Sci 27:1561–1577

Lateef A, Akande MA, Ojo SA, Folarin BI, Gueguim-Kana EB, Beukes LS (2016b) Paper wasp nest-mediated biosynthesis of silver nanoparticles for antimicrobial, catalytic, anti-coagulant and thrombolytic applications. 3 Biotech 6:140

Lateef A, Akande MA, Azeez MA, Ojo SA, Folarin BI, Gueguim-Kana EB, Beukes LS (2016c) Phytosynthesis of silver nanoparticles (AgNPs) using miracle fruit plant (*Synsepalum dulcificum*) for antimicrobial, catalytic, anti-coagulant and thrombolytic applications. Nanotechnol Rev 5:507–520

Lateef A, Azeez MA, Asafa TB, Yekeen TA, Akinboro A, Oladipo IC, Azeez L, Ojo SA, Gueguim-Kana EB, Beukes LS (2016d) Cocoa pod husk extract-mediated biosynthesis of silver nanoparticles: its antimicrobial, antioxidant and larvicidal activities. J Nanostruct Chem 6:159–169

Lateef A, Ojo SA, Elegbede JA (2016e) The emerging roles of arthropods and their metabolites in the green synthesis of metallic nanoparticles. Nanotechnol Rev 5:601–622

Lateef A, Ojo SA, Azeez MA, Asafa TB, Yekeen TA, Akinboro A, Oladipo IC, Gueguim-Kana EB, Beukes LS (2016f) Cobweb as novel biomaterial for the green and eco-friendly synthesis of silver nanoparticles. Appl Nanosci 6:863–874

Lateef A, Ojo SA, Elegbede JA, Azeez MA, Yekeen TA, Akinboro A (2017) Evaluation of some biosynthesized silver nanoparticles for biomedical applications: hydrogen peroxide scavenging, anti-coagulant and thrombolytic activities. J Clust Sci 28:1379–1392

Li SQ, Zhu RR, Zhu H, Xue M, Sun XY, Yao SD, Wang SL (2008) Nanotoxicity of TiO_2 nanoparticles to erythrocyte in vitro. Food Chem Toxicol 46:3626–3631

Li X, Xiao W, He G, Zheng W, Yu N, Tan M (2012) Pore size and surface area control of MgO nanostructures using a surfactant-templated hydrothermal process: high adsorption capability to azo dyes. Colloids Surf A 408:79–86

Lu S, Duffin R, Poland CD, Paul Murphy F, Drost E, MacNee W, Stone V, Donaldson K (2009) Efficacy of simple short-term *in vitro* assays for predicting the potential of metal oxide nanoparticles to cause pulmonary inflammation. Environ Health Perspect 117:241

Lyu J, Zhu L, Burda C (2014) Considerations to improve adsorption and photocatalysis of low concentration air pollutants on TiO_2. Catal Today 225:24–33

Mahmoud HR, Ibrahim SM, El-Molla SA (2015) Textile dye removal from aqueous solutions using cheap MgO nanomaterials: adsorption kinetics, isotherm studies and thermodynamics. Adv Powder Technol. https://doi.org/10.1016/j.apt.2015.12.006

Majumdar SS, Das SK, Chakravarty R, Saha T, Bandyopadhyay TS, Guha AK (2015) A study on lead adsorption by *Mucor rouxii* biomass. Desalination 251:96–102

Mittal A, Kurup L, Mittal I (2007) Freundlich and Langmuir adsorption isotherms and kinetics for the removal of Tartrazine from aqueous solutions using hen feathers. J Hazard Mater 146:243–248

Ojo SA, Lateef A, Azeez MA, Oladejo SM, Akinwale AS, Asafa TB, Yekeen TA, Akinboro A, Oladipo IC, Gueguim-Kana EB, Beukes LS (2016) Biomedical and catalytic applications of gold and silver-gold alloy nanoparticles biosynthesized using cell-free extract of *Bacillus safensis* LAU 13: antifungal, dye degradation, anti-coagulant and thrombolytic activities. IEEE Trans Nanobiosci 15:433–442

Okewale AO, Babayemi KA, Olalekan AP (2013) Adsorption isotherms and kinetics models of starchy adsorbents on uptake of water from ethanol–water systems. Int J Appl Sci Technol 3:35–42

Oladipo IC, Lateef A, Elegbede JA, Azeez MA, Asafa TB, Yekeen TA, Akinboro A, Gueguim-Kana EB, Beukes LS, Oluyide TO, Atanda OR (2017) *Enterococcus* species for the one-pot biofabrication of gold nanoparticles: characterization and nanobiotechnological applications. J Photochem Photobiol B Biol 173:250–257

Olajire AA, Abidemi JJ, Lateef A, Benson NU (2017) Adsorptive desulphurization of model oil by Ag nanoparticles-modified activated carbon prepared from brewer's spent grains. J Environ Chem Eng 5:147–159

Pal J, Deb MK (2014) Efficient adsorption of congo red dye from aqueous solution using green synthesized coinage nanoparticles coated activated carbon beads. Appl Nanosci 4:967–978

Patlolla A, Patlolla B, Tchounwou P (2010) Evaluation of cell viability, DNA damage and cell death in normal human dermal fibroblast cells induced by functionalized multiwalled carbon nanotube. Mol Cell Biochem 338:225–232

Pavya T, Praseetha PK, RimalIsaac RS (2016) Green synthesis of gold nanoparticles using plant sources for cancer therapy: a review. Res J Pharm Biol Chem Sci 7:472–480

Ramalingam B, Khan MMR, Mondal B, Mandal AB, Das SK (2015) Facile synthesis of silver nanoparticles decorated magnetic-chitosan microsphere for efficient removal of dyes and microbial Contaminants. ACS Sustain Chem Eng 3:2291–2302

Sadaf S, Bhatti HN (2014) Evaluation of peanut husk as a novel, low cost biosorbent for the removal of Indosol Orange RSN dye from aqueous solutions: batch and fixed bed studies. Clean Techn Environ Policy 16(3):527–544

Sadhukhan B, Mondal NK, Chattoraj S (2014) Biosorptive removal of cationic dye from aqueous system: a response surface methodological approach. Clean Technol Environ Policy 16:1015–1025

Salehi R, Arami M, Mahmoodi NM, Bahrami H, Khorramfar S (2010) Novel biocompatible composite (Chitosan–zinc oxide nanoparticle): preparation, characterization and dye adsorption properties. Colloids Surf B 80:86–93

Samiey B, Farhadi S (2013) Kinetics and thermodynamics of adsorption of fuchsin acid on nickel oxide nanoparticles. Acta Chim Slov 60:763–773

Santhi M, Kumar PE (2015) Adsorption of Rhodamine B from an aqueous solution: kinetic, equilibrium and thermodynamic studies. Int J Innov Res Sci Eng Technol 4:497–510

Satapanajaru T, Chompuchan C, Suntornchot P, Pengthamkeerati P (2011) Enhancing decolorization of Reactive Black 5 and Reactive Red 198 during nanozerovalent iron treatment. Desalination 266:218–230

Satapathy MK, Banerjee P, Das P (2013) Plant-mediated synthesis of silver-nanocomposite as novel effective azo dye adsorbent. Appl Nanosci 5:1–9

Shen J, Wu Y, Zhang B, Li F (2015) Adsorption of Rhodamine B dye by biomimetic mesoporous SiO_2 nanosheets. Clean Technol Environ Policy 17:2289–2298

Shukla AK, Iravani S (2017) Metallic nanoparticles: green synthesis and spectroscopic characterization. Environ Chem Lett 15:223. https://doi.org/10.1007/s10311-017-0618-2

Sulistina DR, Ratnawati R, Wiyasa IA (2014) Rhodamine B increases hypothalamic cell apoptosis and disrupts hormonal balance in rats. Asian Pac J Reprod 3(3):180–183

Tan IAW, Hameed BH (2010) Adsorption isotherms, kinetics, thermodynamics and desorption studies of basic dye on activated carbon derived from oil palm empty fruit bunch. J Appl Sci 10:2565–2571

Tan KB, Vakili MT, Horri BA, Poh PE, Abdullah AZ, Salamatinia B (2015) Adsorption of dyes by nanomaterials: recent developments and adsorption mechanisms. Separ Purif Technol 150:229–242

Tempkin MI, Pyzhev V (1940) Kinetics of ammonia synthesis on promoted iron catalyst. Acta Phys Chim USSR 12:327–356

Torres MA, Beppu MM, Santana CC (2007) Characterization of chemically modified chitosan microspheres as adsorbents using standard proteins (bovine serum albumin and lysozyme). Braz J Chem Eng 24:325–336

Vanaja M, Paulkumar K, Baburaja M, Rajeshkumar S, Gnanajobitha G, Malarkodi C, Sivakavinesan M, Annadurai G (2014) Degradation of methylene blue using biologically synthesized silver nanoparticles. Bioinorg Chem Appl. https://doi.org/10.1155/2014/742346

Vijayakumar G, Tamilarasan R, Dharmendirakumar M (2012) Adsorption, Kinetic, Equilibrium and Thermodynamic studies on the removal of basic dye Rhodamine-B from aqueous solution by the use of natural adsorbent perlite. J Mater Environ Sci 3:157–170

Xu B (2010) Adsorption behaviour of metal cations on gold nanoparticle surfaces studied by isothermal titration microcalometry. J Chin Chem Soc 57:309–315

Yang K, Xing B (2010) Adsorption of organic compounds by carbon nanomaterials in aqueous phase: Polanyi theory and its application. Chem Rev 110:5989–6008

Zhao J, Xu L, Zhang T, Ren G, Yang Z (2009) Influences of nanoparticle zinc oxide on acutely isolated rat hippocampal CA3 pyramidal neurons. Neurotoxicol 30:220–230